ACS APPLIED MATERIALS & INTERFACES

Letter

www.acsami.org

Surface Complexation-Based Biocompatible Magnetofluorescent Nanoprobe for Targeted Cellular Imaging

Satyapriya Bhandari,[†] Rumi Khandelia,[†] Uday Narayan Pan,[†] and Arun Chattopadhyay*[,†,‡]

[†]Department of Chemistry and [‡]Centre for Nanotechnology, Indian Institute of Technology Guwahati, Guwahati 781039, Assam, India

Supporting Information

ABSTRACT: We report the synthesis of a magnetofluorescent biocompatible nanoprobe—following room temperature complexation reaction between Fe_3O_4—ZnS nanocomposite and 8-hydroxyquinoline (HQ). The composite nanoprobe exhibited high luminescence quantum yield, low rate of photobleaching, reasonable excited-state lifetime, luminescence stability especially in human blood serum, superparamagnetism and no apparent cytotoxicity. Moreover, the nanoprobe could be used for spatio-controlled cell labeling in the presence of an external magnetic field. The ease of synthesis and cell labeling in vitro make it a suitable candidate for targeted bioimaging applications.

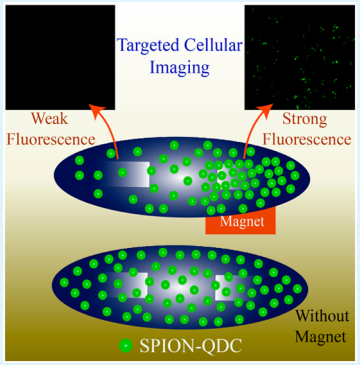

KEYWORDS: *magnetic nanoparticle, quantum dots, photoluminescence, complexation reaction, targeted cellular imaging*

Multifunctional nanostructures, with potential for synergy of action of their components, are an emerging class of materials being proposed, over unifunctional entities, for simultaneous targeting, imaging, and therapeutic applications in the field of biomedical science.[1−10] Among others, magnetofluorescent bifunctional units, such as superparamagnetic iron oxide nanoparticle (SPION)—quantum dot (Qdot) composites, are popular choice in targeted bioimaging.[1−10] The superparamagnetism of SPIONs is useful for magnetic resonance imaging (MRI) in vivo and for targeting tissues guided by an external magnetic field.[1−11] On the other hand, Qdots are preferred over traditional organic dyes in cellular and in vivo imaging because of their unique optical properties, especially photostability, large Stokes-shifted emission, and size-tunable luminescence.[1−13] Thus, a combination of the two, i.e., SPION—Qdot composite, would provide the best of both options. However, concerns regarding cytotoxicity of (especially heavy metal based) Qdots, their dispersibility in aqueous medium, low luminescence quantum yield (QY), ease of functionalization for targeted delivery, stability in blood and circulation lifetime (even for the composite) have limited their application potential.[1−13] For example, the use of Fe_3O_4—ZnS SPION—Qdot composite has been restricted because of low luminescence QY, which makes optical imaging difficult in the presence of cellular autofluorescence.[14,15]

Surface functionalization of the nanocrystals with appropriate ligand or compound may hold the key to colloidal and circulation stability, targeted delivery and even improvement in QY through passivation or other means.[16,17] Recent results from our laboratory suggest that reaction of a molecule/ligand with the cations on the surface of a Qdot leads to drastic change in its optical property via the formation of complex on the surface, referred to as quantum dot complex (QDC). As a result, optical properties (such as emission maximum, QY and excited state lifetime), colloidal and thermal stabilities of the Qdot are greatly improved.[18−21] If the idea could be extended to the magnetofluorescent composite, then their practical utility could be enhanced using some of the properties mentioned above.

Herein we report the formation of a magnetofluorescent composite, based on the complexation reaction between as-synthesized Fe_3O_4—ZnS (SPION—Qdot) composite and 8-hydroxyquinoline (HQ), and referred to here as SPION—QDC composite. The composite particles exhibited superior optical property with red-shifted emission maximum, in comparison to the parent SPION—Qdot, and without the loss of magnetic property or morphology. Furthermore, the stability in human blood serum and non-cytotoxicity made it an important candidate for cellular imaging. Importantly, spatially directed luminescent labeling of mammalian cancer cells (in cell culture Petri plate) could be achieved in the presence of an external magnetic field, thus providing evidence for potential application in targeted delivery.

Experimentally, cysteine-capped Fe_3O_4—ZnS composite was synthesized using 7.3 ± 2.3 nm water-dispersible Fe_3O_4 NP (which was synthesized on the basis of the modification of reported protocols)[22−24] as seed and onto which cysteine-

Received: May 9, 2015
Accepted: July 30, 2015
Published: July 30, 2015

DOI: 10.1021/acsami.5b04022
ACS Appl. Mater. Interfaces 2015, 7, 17552−17557

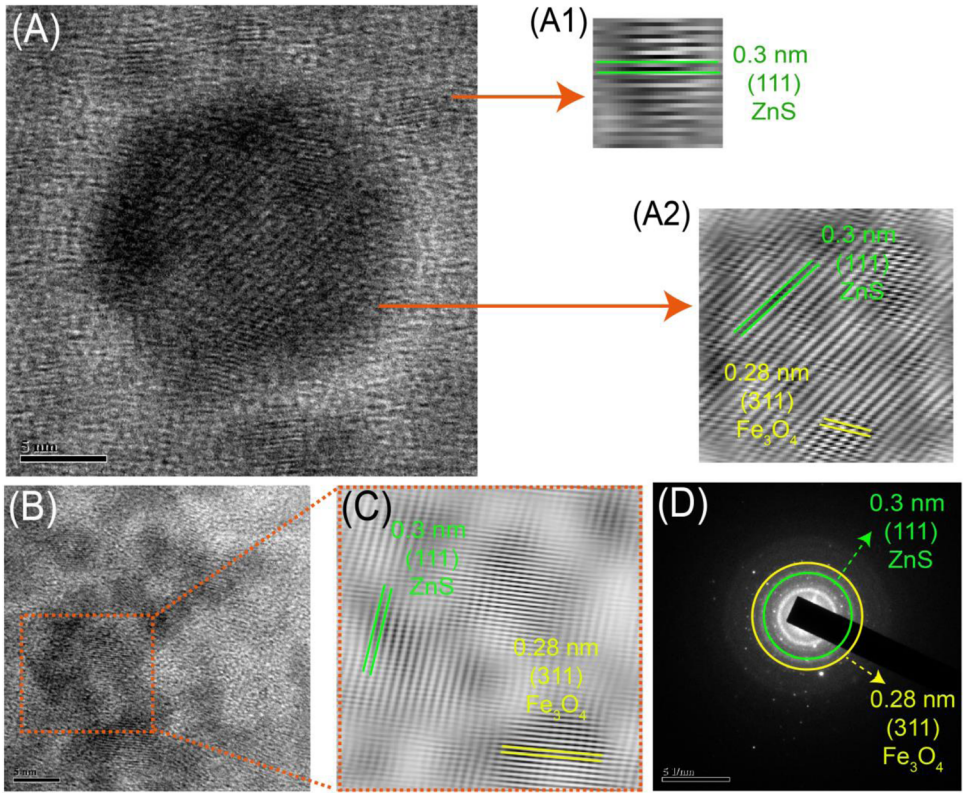

Figure 1. (A) High-resolution TEM (HRTEM; scale bar-5 nm), (1, 2) corresponding inverse fast Fourier transform (IFFT) images of Fe_3O_4–ZnS composite obtained following focusing on the Fe_3O_4 NP, which had size greater than 10 nm, so that 3.2 nm ZnS Qdots could easily be observed simultaneously; (B) high-resolution TEM (HRTEM; scale bar 5 nm) and (C) corresponding inverse fast Fourier transform (IFFT) images of the Fe_3O_4–ZnS composite obtained following focusing on another zone, where Fe_3O_4 NPs and ZnS Qdots were of similar sizes; (D) selected area electron diffraction (SAED) pattern (scale bar 5 nm^{-1}) of the Fe_3O_4–ZnS composite (corresponding to the image in B).

capped ZnS Qdots were grown, based on an earlier method,[21] the details of which are in the experimental section of the Supporting Information. The transmission electron microscopic (TEM) and high-resolution TEM (HRTEM) images confirmed the formation of 7.3 ± 2.3 nm cubic inverse spinel Fe_3O_4 NPs (Figure S1). The powder X-ray diffraction (XRD) pattern of the solid Fe_3O_4–ZnS composite (obtained following magnetic separation) showed the presence of the characteristic peaks of cubic inverse spinel Fe_3O_4 with diffractions at 35.6, 45.2, 53.5, 60.4, and 66.2°, corresponding to (311), (400), (422), (511), and (440) planes and cubic ZnS with diffractions at 28.8, 48.2, and 57.0°, corresponding to (111), (220), and (311) planes, thus confirming the formation of the composite material (Figure S2).[21−25] Also, as is clear from the high-resolution TEM image, 3.2 ± 0.6 nm ZnS Qdots were formed surrounding the Fe_3O_4 NPs (Figure 1A). It is to be mentioned here that the high resolution TEM image and the inverse fast Fourier transform (IFFT) patterns in Figure 1A evidenced the presence of ZnS Qdots surrounding the Fe_3O_4 NPs (>10 nm). Interestingly, the presence of cross pattern, which occurred due to the overlap of lattice fringes of (311) plane of inverse spinel Fe_3O_4 NPs (0.28 nm) and (111) plane of cubic ZnS Qdots (0.3 nm) (Figure 1A–C), clearly indicated the presence of both the crystals in the Fe_3O_4–ZnS composite.[21−25] Importantly, the closeness of the lattice spacing of ZnS Qdot with that of cubic inverse spinel Fe_3O_4 NP might have favored fusion of the Qdot on the NP. Additionally, literature report suggests formation of amorphous overlayer of ZnS on the Fe_3O_4 NP surface prior to fusion of the Qdot with the NP.[14] In a similar vein, the selected area electron diffraction (SAED) analysis of the composite also supported the presence of both the crystals (Figure 1 D). The growth of ZnS nanocrystals on the surface of the Fe_3O_4 NPs was accompanied by the change in zeta potential from −52.0 ± 0.5 mV (for Fe_3O_4 NPs) to −31.1 ± 0.1 mV (for the composite, Table S1).

The aqueous dispersion of Fe_3O_4–ZnS composite upon complexation reaction with HQ (refer to the Supporting Information) exhibited a strong green luminescent color (Figure 2A), following irraditaion with UV (365 nm) light. This was in contrast to the as-synthesized Fe_3O_4–ZnS composite and Fe_3O_4 NPs, which showed no such emission (Figure S3). On the other hand, dispersions of Fe_3O_4 NPs and Fe_3O_4–ZnS composite (following HQ treatment too) were dark and light brown color, respectively, in daylight (Figures S3 and 2A). Importantly, the product of the reaction could be separated using a magnet (Figure 2A) and could again be redispersed in water with retention of luminescence (not shown).

The UV–vis spectrum of the composite following complexation consisted of an excitonic peak at 320 nm (due to the Qdot) and a peak at 365 nm, assigned to ZnQ_2 complex formed on the surface of the Qdot (Figure 2B).[18−21] The luminescence spectrum of the Fe_3O_4–ZnS composite consisted of a broad emission centered at 440 nm (upon excitation at 320 nm; Figure 2C), which occurred possibly because of the coupling of surface defect states with the core state of the ZnS Qdots.[26,27] On the other hand, following complexation the emission peak at 440 nm disappeared and a new and intense

DOI: 10.1021/acsami.5b04022
ACS Appl. Mater. Interfaces 2015, 7, 17552−17557

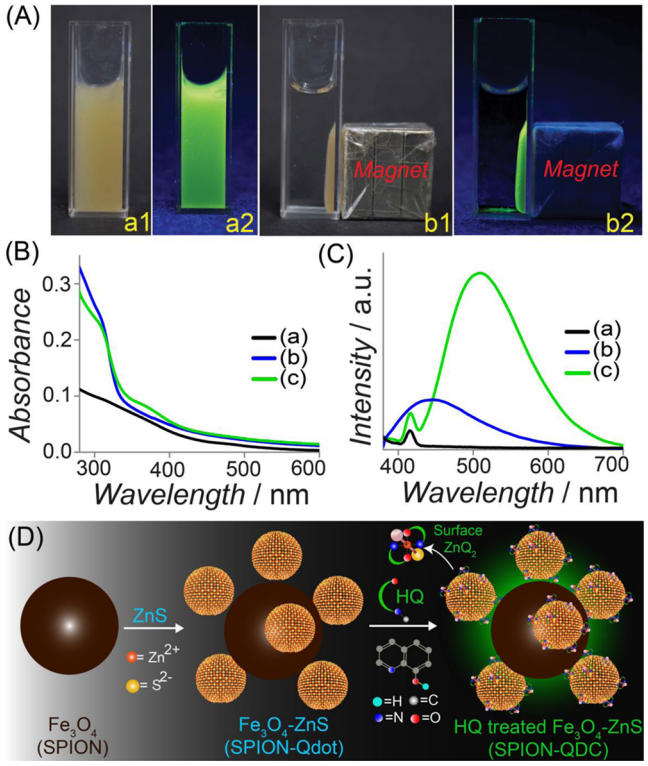

Figure 2. (A) Photographs of the aqueous dispersion of SPION−QDC in the (a) absence and (b) presence of an external magnetic field under (1) white and (2) UV light (365 nm). (B) UV−vis and (C) emission spectra of the aqueous dispersion of (a) Fe_3O_4 (pH 9.5; λ_{ex}, 320 nm); (b) Fe_3O_4−ZnS (pH 6.8; λ_{ex}, 320 nm); and (c) SPION−QDC (pH 6.8; λ_{ex}, -365 nm). (D) Schematic representation of the formation of SPION−QDC composite.

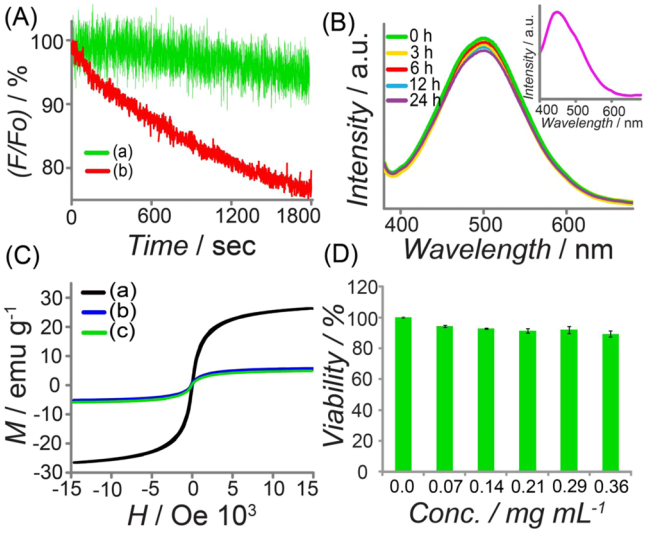

Figure 3. (A) Photostability (λ_{ex}, 365 nm) under continuous irradiation of light of (a) SPION−QDC (in water; λ_{em}, 500 nm) and (b) rhodamine 6G organic dye (in ethanol; λ_{em}, 570 nm). (B) Luminescence (λ_{ex}, 365 nm) stability of SPION−QDC composite in human blood serum as measured at different time intervals; Inset: emission spectrum (λ_{ex}, 365 nm) of only human blood serum. (C) *M*−*H* hysteresis curves of the solid particles of (a) Fe_3O_4, (b) Fe_3O_4−ZnS (SPION−Qdot), and (c) SPION−QDC. (D) MTT-based cell viability assay of HeLa cells after 24 h treatment with varying concentrations of SPION−QDC composite.

emission peak appeared at 500 nm (Figure 2C). The excitation maximum for the peak at 500 nm appeared at 365 nm (Figure S4). The results are consistent with previous observations of formation of ZnQ_2 complex on the surface of ZnS Qdot.[18−21] However, Fe_3O_4 nanocrystals did not have any clear emission peak even in the presence of HQ, thus discounting the possibility of the peak at 500 nm due to any product (associated with Fe) from the reaction (Figure S5). It is to be mentioned here that the formed surface ZnQ_2 complexes act as quencher of the Qdot emission and the green emission of the attached ZnQ_2 complex to Qdot originates because of the electronic transition from the electron-rich phenoxide ring (HOMO; highest occupied molecular orbital) to the electron deficient pyridyl ring (LUMO; lowest unoccupied molecular orbital) of HQ moiety of the surface attached ZnQ_2 complexes.[18−21] Overall, the results suggest that several ZnS nanocrystals grew on each Fe_3O_4 (although, considering the similarity of the crystal sizes smaller number of attached ZnS crystals per Fe_3O_4 particle cannot be ruled out); the complexation reaction led to the formation of ZnQ_2 on the surface of the ZnS Qdots. Earlier results suggested the bonding of the complex with the dangling sulfide ions present on the surface, whereas the sixth coordinate may be occupied by H_2O and the attached ZnQ_2 complexes provide the chemical stability and solubilty to the composite.[18−21] We define the new composite as SPION−QDC (SPION−Qdot complex), the formation of which is schematically shown in Figure 2D. It is to be mentioned here that the optimum amount of HQ required for the reaction was calculated by monitoring the saturation in emission intensity at 500 nm (Figure S6A). It was found to require 0.03 mM HQ for a 2.0 mL of Fe_3O_4−ZnS composite dispersion (with an absorbance value of 0.20−0.25 at 320 nm). That the luminescence at 500 nm was due to the formaton of a complex was further supported by the retention of emission following centrifugation of the product and redispersion into the same medium (Figure S6B). Furthermore, there was no significant change in pH of the reaction medium after complexation, which ruled out the effect of pH on the changes in the luminescence.

Fourier transform infrared (FTIR) spectroscopy results showed that SPION−QDC contained the functional groups corresponding to the octahedral ZnQ_2 complexes, which were absent in Fe_3O_4−ZnS (SPION−Qdot) composite.[18−21] The details are described in the Figure S7. Additionally, the elemental analysis, from atomic absorption spectroscopy (AAS), showed constancy of Fe:Zn content, thus indicating that there was no discernible depletion of metal ions from the composite due to complexation reaction (Table S2). However, the changes in the zeta potential indicated modification of the SPION−Qdot surface following complexation (Table S1). Also, the preservation of morphological characteristics of the Fe_3O_4−ZnS composite following complexation with HQ was confirmed by XRD, TEM, and SAED analyses (Figure S8−S9).[21−25]

The as-synthesized Fe_3O_4−ZnS (SPION−Qdot) composite had a photoluminescence QY of 0.6% (at 320 nm excitation). On the other hand, the SPION−QDC resulted in a QY of 5.9% (with excitation at 365 nm) and 0.8% (with excitation at 320 nm, Table S3). The significant enhancement of QY and the red-shift of the excitation maximum, due to the formation of complex on the surface of Qdot is expected to make the SPION−QDC more attractive for bioimaging, especially against the background of strong cellular autofluorescence.[13,28]

DOI: 10.1021/acsami.5b04022
ACS Appl. Mater. Interfaces 2015, 7, 17552−17557

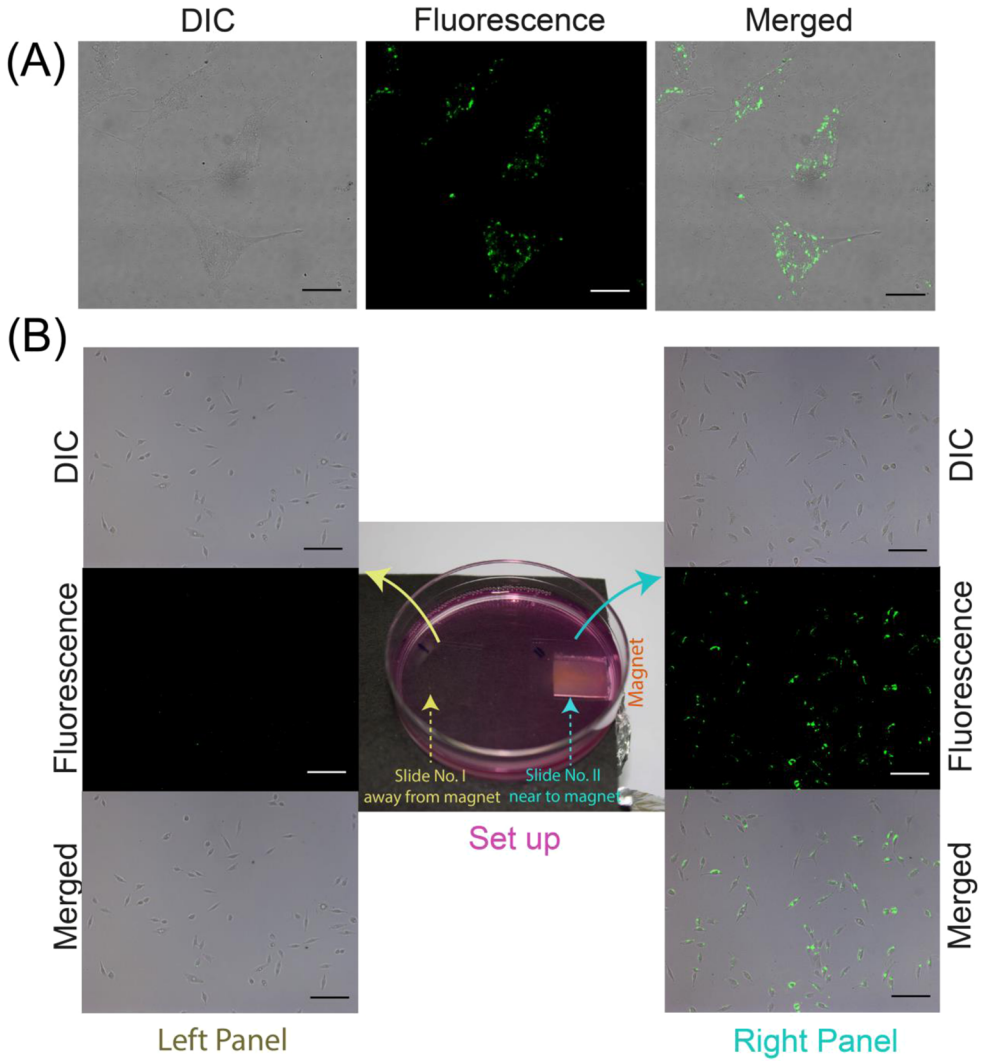

Figure 4. (A) Confocal laser scanning microscopic images (scale bar -25 μm) of HeLa cells following 4 h incubation with SPION−QDC. (B) Fluorescence microscopic images (scale bar 100 μm) of HeLa cells, which were cultured on two coverslips placed inside a Petri plate and incubated with SPION−QDC for 4 h. A magnet was placed below one coverslip during incubation. The images are for cells on the coverslip (I) away from the external magnet (left panel) and (II) the other one closer to magnet (right panel). The image for the setup is in the second column.

Additionally, the average excited-state lifetime of the SPION−QDC was measured to be 12.54 ns, also enhancing their potential for bioimaging (Figure S10 and Table S4).[18] Furthermore, the HQ treated Fe_3O_4−ZnS composite was found 5 times more photostable than an organic dye (here rhodamine 6G). For example, the decrease in luminescence intensity for HQ treated Fe_3O_4−ZnS and rhodamine 6G were observed to be 0.003 and 0.014% per sec (Figure 3A and Table S5), supporting the superiority of the composite. Moreover, the stability of the luminescence (at λ_{ex}-365 nm and λ_{em}-500 nm) of the SPION−QDC in human blood serum (as measured for 24 h) indicated its clinical application potential (Figure 3B). Additionally, the zeta potential of the aqueous dispersion of the SPION−QDC was measured to be −25.5 ± 0.6 mV, indicating its colloidal stability in water, which is required for biological applications (Table S1).[18−21] Furthermore, the stability and long-term storage in solid forms were confirmed by preservation of the bright green fluorescence, even after 15 days, as observed under fluorescence microscope (Figure S11).

The vibrating sample magnetometric (VSM) analysis of Fe_3O_4, Fe_3O_4−ZnS, and SPION−QDC showed magnetization saturation values of 26.4, 3.88, and 3.81 emu/g, respectively and the measurements supported their superparamagnetic nature at room temperature (Figure 3C and Table S6).[3,14,15] The decrease in magnetic saturation of Fe_3O_4−ZnS composite compared to Fe_3O_4 NPs (per unit weight) may be due to the diamagnetic ZnS nanocrystals formed surrounding the Fe_3O_4 NPs.[14] Additionally, the treatment of HQ to Fe_3O_4−ZnS composite did not significantly change its magnetic saturation. Furthermore, the SPION−QDC showed magnetic saturation value of 3.81, which is sufficient for magnet guided imaging applications.[3] The MTT-based cell viability assay, performed using different concentrations (with a maximum 0.36 mg/mL) of the SPION−QDC, showed that more than 90% of the cervical cancer HeLa cells were viable after 24 h of incubation (Figure 3D). This clearly indicated that the composite was nontoxic to the mammalian cells and thus makes it suitable for biological applications.

Additionally, the SPION−QDC composite exhibited bright green luminescence under confocal microscope, using 405 nm diode laser (Figure 4A), whereas no such green fluorescence was observed in control HeLa cells (Figure S12). Importantly,

DOI: 10.1021/acsami.5b04022
ACS Appl. Mater. Interfaces 2015, 7, 17552−17557

the magnetic property of the composite offered the opportunity for labeling of cells with spatial control, by using external magnetic field. In order to achieve this, HeLa cells were cultured onto two coverslips, placed inside a cell culture Petri plate, and then incubated with the SPION−QDC composite for 4 h. A small magnet was placed below the Petri plate and closer to one of the coverslips (Figure 4B). When viewed using a microscope, strong green luminescence was observed for the cells on the coverslip which was near to magnet (Figure 4B; right panel), whereas the cells on the other one (away from the magnet) showed negligible luminescence (Figure 4B; left panel). On the other hand, in the absence of any magnet strong green luminescence from the cells attached to both the coverslips could be observed (Figure S13). This means that the magnetic property of the composite could be used to direct the same for cell labeling with spatial control. This may auger well for targeted cellular imaging and drug delivery.

In conclusion, a new composite has been developed on the basis of the complexation reaction of Fe_3O_4−ZnS composite nanocrystals with HQ, leading to the formation of luminescent ZnQ_2 on the surface of the Qdot. The high photoluminescence QY, photostability and superparamagnetism of the SPION−QDC composite were used to demonstrate cellular labeling with spatial control using an external magnetic field. Furthermore, the luminescence stability in human blood serum, nontoxicity and magnet guided specific cell imaging properties of the biocompatible SPION−QDC would make it a suitable candidate for targeted bioimaging. Moreover, the complexation-based QY enhancement of multifunctional materials can be expected to bring new excitement in biodiagnostics in near future.

■ ASSOCIATED CONTENT

Supporting Information

. The Supporting Information is available free of charge on the ACS Publications website at DOI: 10.1021/acsami.5b04022.

Experimental details, synthesis and characterization of Fe_3O_4 nanoparticles, Fe_3O_4−ZnS (SPION−Qdot) composite, HQ-treated Fe_3O_4−ZnS (SPION−QDC) composite, fluorescence images of HeLa cells incubated with SPION−QDC composite (in absence of magnetic field), Figures S1−S14, and Tables S1−S6 (PDF)

■ AUTHOR INFORMATION

Corresponding Author

*E-mail: arun@iitg.ernet.in.

Notes

The authors declare no competing financial interest.

■ ACKNOWLEDGMENTS

We thank the Department of Electronics and Information Technology (5(9)/2012-NANO (Vol. II)), Government of India, for fund. Assistances from CIF, IIT Guwahati, Shilaj Roy, Sabyasachi Pramanik, Dr. Anupam Banerjee, Dr. Subhojit Das, Amaresh Kumar Sahoo, Partha Maity, and Puspal Mukherjee are acknowledged. S.B. and R. K. thank the CSIR for fellowships (09/731(0115)/2011-EMR-I, 09/731(0105)/2010-EMR-I).

■ REFERENCES

(1) Chen, O.; Riedemann, L.; Etoc, F.; Herrmann, H.; Coppey, M.; Barch, M.; Farrar, C. T.; Zhao, J.; Bruns, O. T.; Wei, H.; Guo, P.; Cui, J.; Jensen, R.; Chen, Y.; Harris, D. K.; Cordero, J. M.; Wang, Z.; Jasanoff, A.; Fukumura, D.; Reimer, R.; Dahan, M.; Jain, R. K.; Bawendi, M. G. Magneto-Fluorescent Core-Shell Supernanoparticles. *Nat. Commun.* **2014**, *5*, 5093−5105.

(2) Ruan, G.; Vieira, G.; Henighan, T.; Chen, A.; Thakur, D.; Sooryakumar, R.; Winter, J. O. Simultaneous Magnetic Manipulation and Fluorescent Tracking of Multiple Individual Hybrid Nanostructures. *Nano Lett.* **2010**, *10*, 2220−2224.

(3) Gao, J.; Zhang, W.; Huang, P.; Zhang, B.; Zhang, X.; Xu, B. Intracellular Spatial Control of Fluorescent Magnetic Nanoparticles. *J. Am. Chem. Soc.* **2008**, *130*, 3710−3711.

(4) Erogbogbo, F.; Yong, K.; Hu, R.; Law, W.; Ding, H.; Chang, C.; Prasad, P. N.; Swihart, M. T. Biocompatible Magnetofluorescent Probes: Luminescent Silicon Quantum Dots Coupled with Superparamagnetic Iron(III) Oxide. *ACS Nano* **2010**, *4*, 5131−5138.

(5) Park, J.; von Maltzahn, G.; Ruoslahti, E.; Bhatia, S. N.; Sailor, M. J. Micellar Hybrid Nanoparticles for Simultaneous Magnetofluorescent Imaging and Drug Delivery. *Angew. Chem., Int. Ed.* **2008**, *47*, 7284−7288.

(6) Di Corato, R.; Bigall, N. C.; Ragusa, A.; Dorfs, D.; Genovese, A.; Marotta, R.; Manna, L.; Pellegrino, T. Multifunctional Nanobeads Based on Quantum Dots and Magnetic Nanoparticles: Synthesis and Cancer Cell Targeting and Sorting. *ACS Nano* **2011**, *5*, 1109−1121.

(7) Gu, H.; Zheng, R.; Zhang, X.; Xu, B. Facile One-Pot Synthesis of Bifunctional Heterodimers of Nanoparticles: A Conjugate of Quantum Dot and Magnetic Nanoparticles. *J. Am. Chem. Soc.* **2004**, *126*, 5664−5665.

(8) Selvan, S. T.; Patra, P. K.; Ang, C. Y.; Ying, J. Y. Synthesis of Silica-Coated Semiconductor and Magnetic Quantum Dots and Their Use in the Imaging of Live Cells. *Angew. Chem., Int. Ed.* **2007**, *46*, 2448−2452.

(9) Cho, M.; Contreras, E. Q.; Lee, S. S.; Jones, C. J.; Jang, W.; Colvin, V. L. Characterization and Optimization of the Fluorescence of Nanoscale Iron Oxide/Quantum Dot Complexes. *J. Phys. Chem. C* **2014**, *118*, 14606−14616.

(10) Jennings, L. E.; Long, N. J. Two Is Better Than One'—Probes for Dual-modality Molecular Imaging. *Chem. Commun.* **2009**, 3511−3524.

(11) Mahmoudi, M.; Hosseinkhani, X. H.; Hosseinkhani, M.; Boutry, S.; Simchi, A.; Journeay, W. S.; Subramani, K.; Laurent, S. Magnetic Resonance Imaging Tracking of Stem Cells in Vivo Using Iron Oxide Nanoparticles as a Tool for the Advancement of Clinical Regenerative Medicine. *Chem. Rev.* **2011**, *111*, 253−280.

(12) Medintz, I. L.; Uyeda, H. T.; Goldman, E. R.; Mattoussi, H. Quantum Dot Bioconjugates for Imaging, Labeling and Sensing. *Nat. Mater.* **2005**, *4*, 435−446.

(13) Mandal, G.; Darragh, M.; Wang, Y. A.; Heyes, C. D. Cadmium-free Quantum Dots as Time-gated Bioimaging Probes in Highly-autofluorescent Human Breast Cancer Cells. *Chem. Commun.* **2013**, *49*, 624−626.

(14) Yu, X.; Wan, J.; Shan, Y.; Chen, K.; Han, X. A Facile Approach to Fabrication of Bifunctional Magnetic-Optical Fe_3O_4@ZnS Microspheres. *Chem. Mater.* **2009**, *21*, 4892−4898.

(15) Wang, Z.; Wu, L.; Chen, M.; Zhou, S. Facile Synthesis of Superparamagnetic Fluorescent Fe_3O_4/ZnS Hollow Nanospheres. *J. Am. Chem. Soc.* **2009**, *131*, 11276−11277.

(16) Huang, J.; Liu, W.; Dolzhnikov, D. S.; Protesescu, L.; Kovalenko, M. V.; Koo, B.; Chattopadhyay, S.; Shenchenko, E. V.; Talapin, D. V. Surface Functionalization of Semiconductor and Oxide Nanocrystals with Small Inorganic Oxoanions (PO_4^{3-}, MoO_4^{2-}) and Polyoxometalate Ligands. *ACS Nano* **2014**, *8*, 9388−9402.

(17) Susumu, K.; Uyeda, H. T.; Medintz, I. L.; Pons, T.; Delehanty, J. B.; Mattoussi, H. Enhancing the Stability and Biological Functionalities of Quantum Dots via Compact Multifunctional Ligands. *J. Am. Chem. Soc.* **2007**, *129*, 13987−13996.

(18) Bhandari, S.; Roy, S.; Pramanik, S.; Chattopadhyay, A. Double Channel Emission from a Redox Active Single Component Quantum Dot Complex. *Langmuir* **2015**, *31*, 551−561.

DOI: 10.1021/acsami.5b04022
ACS Appl. Mater. Interfaces 2015, 7, 17552−17557

(19) Bhandari, S.; Roy, S.; Pramanik, S.; Chattopadhyay, A. Surface Complexation Reaction for Phase Transfer of Hydrophobic Quantum Dot from Nonpolar to Polar Medium. *Langmuir* **2014**, *30*, 10760−10765.
(20) Pramanik, S.; Bhandari, S.; Roy, S.; Chattopadhyay, A. Synchronous Tricolor Emission-Based White Light from Quantum Dot Complex. *J. Phys. Chem. Lett.* **2015**, *6*, 1270−1274.
(21) Bhandari, S.; Roy, S.; Chattopadhyay, A. Enhanced Photoluminescence and Thermal Stability of Zinc Quinolate Following Complexation on the Surface of Quantum Dot. *RSC Adv.* **2014**, *4*, 24217−24221.
(22) Xu, Z.; Hou, Y.; Sun, S. Magnetic Core/Shell Fe_3O_4/Au and Fe_3O_4/Au/Ag Nanoparticles with Tunable Plasmonic Properties. *J. Am. Chem. Soc.* **2007**, *129*, 8698−8699.
(23) Park, J. N.; An, K. J.; Hwang, Y. S.; Park, J. G.; Noh, H. J.; Kim, J. Y.; Park, J. H.; Hwang, N. M.; Hyeon, T. W. Ultra-Large-Scale Syntheses of Monodisperse Nanocrystals. *Nat. Mater.* **2004**, *3*, 891.
(24) Euliss, L. E.; Grancharov, S. G.; O'Brien, S.; Deming, T. J.; Stucky, G. D.; Murray, C. B.; Held, G. A. Cooperative Assembly of Magnetic Nanoparticles and Block Copolypeptides in Aqueous Media. *Nano Lett.* **2003**, *3*, 1489−1493.
(25) Beltran-Huarac, J.; Guinel, M. J-F.; Weiner, B. R.; Morell, G. Bifunctional Fe_3O_4/ZnS:Mn Composite Nanoparticles. *Mater. Lett.* **2013**, *98*, 108−111.
(26) Kambhampati, P. On the Kinetics and Thermodynamics of Excitons at the Surface of Semiconductor Nanocrystals: Are There Surface Excitons? *Chem. Phys.* **2015**, *446*, 92−107.
(27) Mooney, J.; Krause, M. M.; Saari, J. I.; Kambhampati, P. Challenge to the Deep-Trap Model of the Surface in Semiconductor Nanocrystals. *Phys. Rev. B: Condens. Matter Mater. Phys.* **2013**, *87*, 081201(R).
(28) Fernandez-Moreira, V.; Thorp-Greenwood, F. L.; Coogan, M. P. Application of d^6 Transition Metal Complexes in Fluorescence Cell Imaging. *Chem. Commun.* **2010**, *46*, 186−202.

DOI: 10.1021/acsami.5b04022
ACS Appl. Mater. Interfaces 2015, 7, 17552−17557